RESEARCH ARTICLE
Editor's Choice
ADVANCED MATERIALS
www.advmat.de

# Fast Encapsulation of Microbes into Dissolvable Hydrogel Beads Enables High-Throughput Microbial Single-Cell RNA Sequencing of Clinical Microbiome Samples

*Yuting Wang, Junjie Ma, Wenjie Cai, Mengdi Song, Zhaolun Wang, Ziye Xu, Yifei Shen, Shufa Zheng, Shunji Zhang, Zhengmin Tang,* and Yongcheng Wang**

**Microbial single-cell RNA-seq (mscRNA-seq) can achieve resolution at the cellular level, enhancing the understanding of microbial communities. However, current high-throughput mscRNA-seq methods are limited by multiple centrifugation steps, which can lead to microbial loss and bias. smGel-seq is reported, a high-throughput single-microbe RNA sequencing method for clinical microbiome samples that employs hydrogel beads to encapsulate individual microbes to reduce microbial loss and input requirements. In this method, a novel microchannel array device is implemented for encapsulating single microbe in dissolvable hydrogel beads (smDHBs), along with an optimized automated microfluidic platform to co-encapsulate barcoded beads and smDHBs, enabling high-throughput barcoding of individual microbes. smGel-seq significantly increases the microbial recovery rate in a gut microbiome sample from 8.8% to 91.8%. Furthermore, this method successfully processes clinical microbiome samples with microbial inputs 20 times lower than those required by previous methods. Notably, smGel-seq enables the first mscRNA-seq in a clinical sputum microbiome sample, revealing a specific microbial subpopulation that may play a key role in environmental adaptability, antibiotic resistance, and pathogenicity. These results highlight the compatibility of smGel-seq with clinical microbiome samples and demonstrate its potential for widespread application in diverse clinical and research settings.**

## 1. Introduction

As integral components of the domains of living organisms, microbes contribute significantly to maintaining the biosphere and regulating human health.[1–4] Microbes within their microbial communities exhibit diverse roles at the strain level, and this microbial heterogeneity leads to complex interactions both within microbial communities and between microbes and their host.[5–7] Metatranscriptome methods based on next-generation sequencing[8] or nanopore sequencing,[9,10] can elucidate the functionality of microbiomes in bulk, but are still limited in revealing the heterogeneity of individual cells.[5] Microbial single-cell RNA sequencing (mscRNA-seq) offers a novel approach for microbiome research by providing transcriptional insights of individual microbes and uncovering functional variations at the single-cell level.[5] To date, mscRNA-seq has demonstrated extensive application in the biomedical field, including the exploration of associations between microorganisms and hosts,[11] microbial drug resistance,[12] and microbial metabolic functions.[13]

Despite its potential, current mscRNA-seq methods face several technical limitations. Existing low-throughput mscRNA-seq methods primarily rely on multi-well plates for single-cell isolation, restricting throughput to hundreds of microbes and offering limited coverage for complex microbial communities.[14,15] Recently developed high-throughput microbial single-cell RNA sequencing methods, such as microSPLiT,[13] PETRI-seq,[16] BacDrop,[12] and smRandom-seq,[17] have optimized methodological approaches to significantly increase cell throughput to the tens of thousands. However, these methods require over 10 centrifugation steps to remove residual reagents after reactions, resulting in substantial microbial loss.[18] This limitation restricts the applicability of mscRNA-seq to samples with low microbial abundance, such as clinical respiratory samples. Moreover, the inherent variation in cell size among microbial species in microbiota (ranging from less than 0.6 µm to over 120 µm)[19,20] leads to inconsistent losses during centrifugation, introducing significant bias.[12,17] These species-specific biases can skew microbial representation in the final data, potentially misleading prognostic evaluations and clinical decisions. Therefore, there is an urgent need to develop a new mscRNA-seq method that provides more accurate

Y. Wang, J. Ma, W. Cai, M. Song, Z. Wang, Z. Xu, Y. Shen, S. Zheng, S. Zhang, Z. Tang, Y. Wang
Department of Laboratory Medicine of The First Affiliated Hospital & Liangzhu Laboratory
Zhejiang University School of Medicine
Hangzhou 311121, China
E-mail: tzhengmin@zju.edu.cn; yongcheng@zju.edu.cn
Y. Wang, S. Zhang, Y. Wang
College of Biomedical Engineering and Instrument Science
Zhejiang University
Hangzhou 310027, China

The ORCID identification number(s) for the author(s) of this article can be found under https://doi.org/10.1002/adma.202500481

DOI: 10.1002/adma.202500481

 

characterization of clinical samples, improves compatibility with low microbial input, and reduces the bias introduced during processing.

Here, we introduce smGel-seq, a high-throughput and low microbial input mscRNA-seq method, which enables the isolation of single microbes within dissolvable hydrogel beads (smDHBs) to mitigate microbial loss and bias. We reported a microchannel array (μCA) device capable of high-throughput droplet generation using a handheld syringe, which enables the efficient generation of smDHBs and significantly reduces the risk of RNA degradation during processing. Additionally, we optimized an automated microfluidic platform for the co-encapsulation of smDHBs and barcoded beads into droplets, facilitating high-throughput barcoding for individual microbes. The smGel-seq led to a substantial increase in the microbial recovery rate of microbiome samples, from 8.8% with smRandom-seq to 91.8%. We applied smGel-seq to clinical microbiome samples with microbial input 20 times lower than that required for smRandom-seq, achieving the first high-throughput mscRNA-seq in a clinical sputum microbiome sample, which was unattainable using previous methods. We successfully identified the pathogenic bacterial species *Acinetobacter baumannii* present in this sputum sample, matching the clinical culture results. In our further analysis, we identified two subpopulations of *Acinetobacter baumannii* in the clinical sputum microbiome sample, one of which exhibited greater environmental adaptation and a stronger role in antibiotic resistance and virulence. This work combines high-throughput capability with low microbial input requirements, demonstrating its potential for future mscRNA-seq applications on clinical microbiome samples with limited cell quantities.

## 2. The Workflow of smGel-seq for High-Throughput mscRNA-seq

The overall concept of smGel-seq is illustrated in **Figure 1**. Initially, microbes were fixed overnight with 4% paraformaldehyde (PFA) to crosslink proteins and nucleic acids. The fixed microbes were then mixed with a polyacrylamide solution containing polyacrylamide monomer and *N,N'*-bis(acryloyl)cystamine (BAC). This mixture was subsequently isolated into water-in-oil droplets using a μCA device (Figure 1a), where the acrylamide monomer reacted with the crosslinker BAC to generate smDHBs by radical polymerization.[21] The porous structure of the smDHBs prevents microbes from escaping the beads while allowing small molecules, including primers, dNTPs, enzymes, and other reagents, to freely diffuse in and out. This encapsulation demonstrated high recovery rates after multiple centrifugation steps, overcoming the significant microbial loss reported during multiple centrifugation steps in previous mscRNA-seq techniques (Figure 1b).[12,13,16,17]

The workflow for smGel-seq library preparation is illustrated in Figure 1c. First, the generated smDHBs were sequentially transferred to different reaction systems for library preparation. In the reverse transcription, random primers penetrated the smDHBs to capture microbial RNA and convert it into cDNA in situ. Subsequently, terminal transferase added a poly(dA) tail to the 3′ end of the cDNA in situ during the dA tailing reaction. After each reaction, smDHBs are centrifuged and washed 3–5 times before proceeding to the next reaction. Following the dA tailing reaction, the smDHBs, DNA extension reagents, and DNA barcoded beads are co-encapsulated into water-in-oil droplets using an automated microfluidic device. Within these droplets, the poly(dT) sequences on the barcoded beads hybridize with the poly(dA) tails of the cDNA ends, enabling barcoding through extension, which distinguishes the transcriptome information of individual microbes. The disulfide bonds in polyacrylamide hydrogel beads can be rapidly cleaved by dithiothreitol (DTT) (Figure 1d).[21] To release the cDNA library, the droplets were broken and smDHBs were dissolved by DTT. Subsequently, the cDNA was purified using magnetic beads and amplified through PCR. The final cDNA library was constructed for high-throughput next-generation sequencing.

The hydrogel encapsulation strategy has been widely utilized across various biological applications, including cell culture,[22] molecular detection,[23,24] secretory profiling,[25] DNA sequencing,[26,27] and eukaryotic single-cell RNA sequencing. However, the application of hydrogel encapsulation in microbial single-cell RNA sequencing has not been developed due to challenges such as microbial loss, RNA degradation, the balance between microbial retention and reagent permeability, and the need for rapid dissolution under mild conditions to release library. To address these issues, we developed a μCA device for rapid generation of smDHBs with optimized permeability, enabling efficient reagent diffusion while retaining microbes and ensuring high library recovery. By integrating μCA device and the optimized hydrogel system, smGel-seq reduced microbial loss and bias during sample processing, making it suitable for clinical samples with low microbial biomass. Notably, our method demonstrates clinical potential by achieving microbial single-cell RNA sequencing of the clinical sputum sample and uncovering functionally significant subpopulations.

## 3. Fast Production of the smDHBs by the μCA Device

The μCA chip is designed for droplet generation through step emulsification, with low shear stress, flow rate insensitivity, and an easily integrable assembly (**Figure 2**a and Figures S1, S2, Supporting Information). The μCA chip consists of a silicon wafer substrate bonded to a glass cover with a cylindrical through-hole. The silicon wafer substrate is patterned with a microchannel array, and 36 groove-type nozzles were etched around its outer edge. When an external pressure is applied to the through-hole of the glass, the aqueous phase flows into the microchannels, and continuously generates continuous droplets at the nozzles. Figure 2b shows the μCA chips fabricated on a silicon wafer. Over 2000 chips can be etched onto a single 6 in. wafer, demonstrating that traditional microfabrication techniques enable large-scale production of μCA chips. A complete μCA device comprises three components: the μCA chip, an aqueous container, and an oil cup (Figure 2c). The aqueous container features a hollowed-out bulge designed to fit into the glass through-hole, ensuring that the aqueous phase does not leak from the junction. The assembly of the μCA device can be easily performed through manual operation without the need for connecting tubing, as previously described (Figure S3, Supporting Information).[28] For droplets generation, the bulge of the aqueous container was inserted into

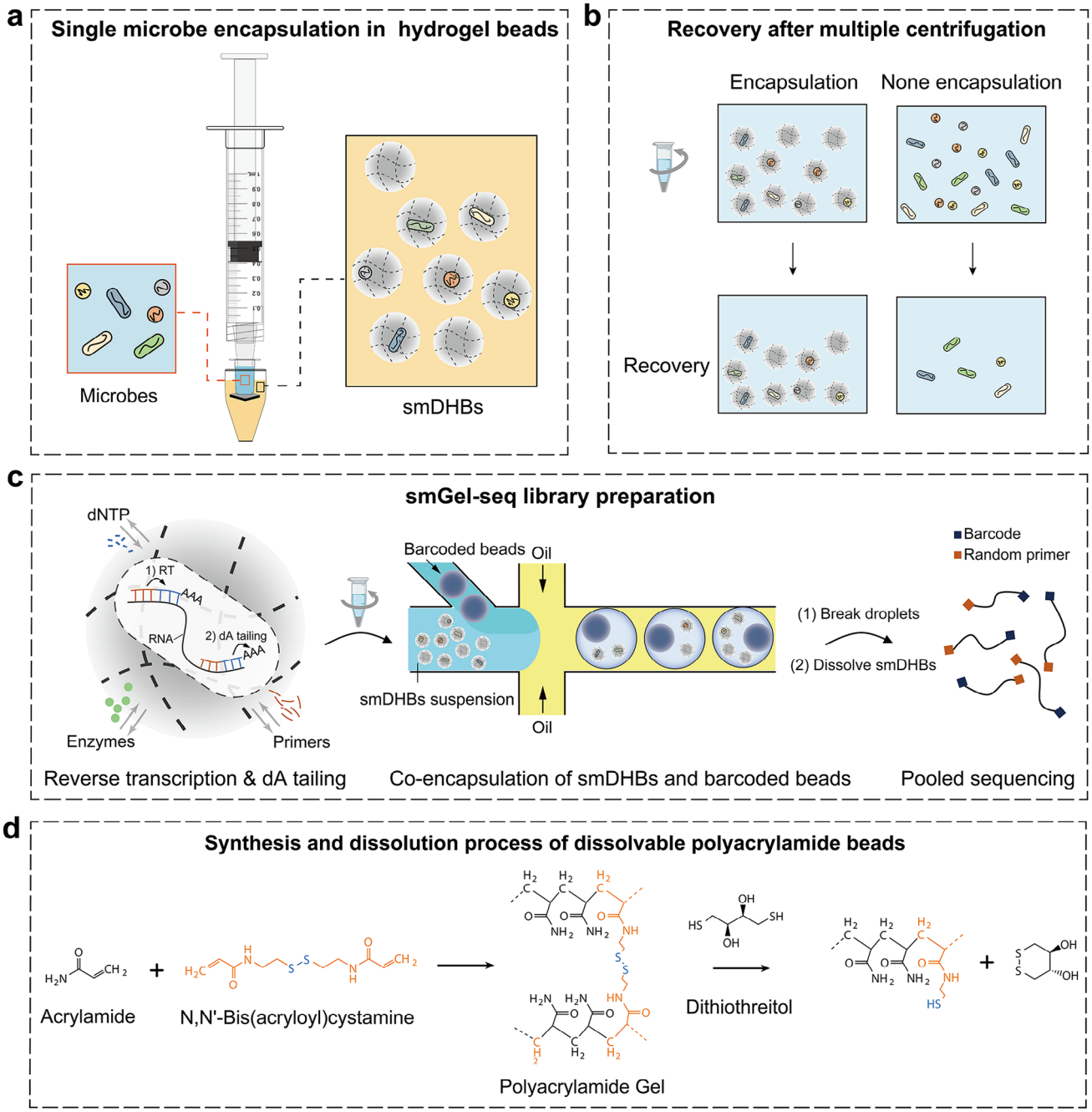


**Figure 1.** The workflow of encapsulating microbiome in dissolvable hydrogel beads for microbial single-cell RNA sequencing. a) A mixture of polyacrylamide solution (polyacrylamide monomer and BAC) and microbes fixed by 4% paraformaldehyde is emulsified with carrier oil by a microchannel array device, resulting in the encapsulation of single microbes in dissolvable hydrogel beads (smDHBs). b) The use of smDHBs improves the recovery rate during centrifugation by introducing uniform mass to the microbes, ensuring better sedimentation and reducing microbial loss. c) For smGel-seq library preparation, smDHBs undergo a series of reactions, including reverse transcription, dA tailing, and co-encapsulation of smDHBs and barcoded beads for droplet barcoding. Then the smDHBs are dissolved after the droplets are broken. The barcoded cDNAs are pooled and prepared for next-generation sequencing. d) Synthesis and dissolution principle of dissolvable polyacrylamide hydrogels.

the through-hole of the μCA chip, and the aqueous container connected to the μCA chip was then placed into an oil cup containing sufficient carrier oil to fully submerge the chip. Finally, a handheld syringe was inserted into the aqueous container to inject the aqueous phase into the chip. Microscopic observations confirm that the generated droplets exhibit high uniformity, meeting the requirements for experimental applications (Figure 2d). Droplet generation using the μCA device is simple and efficient, enabling the rapid production of 10 million droplets within 30 s, which is much fast and convenient than traditional PDMS

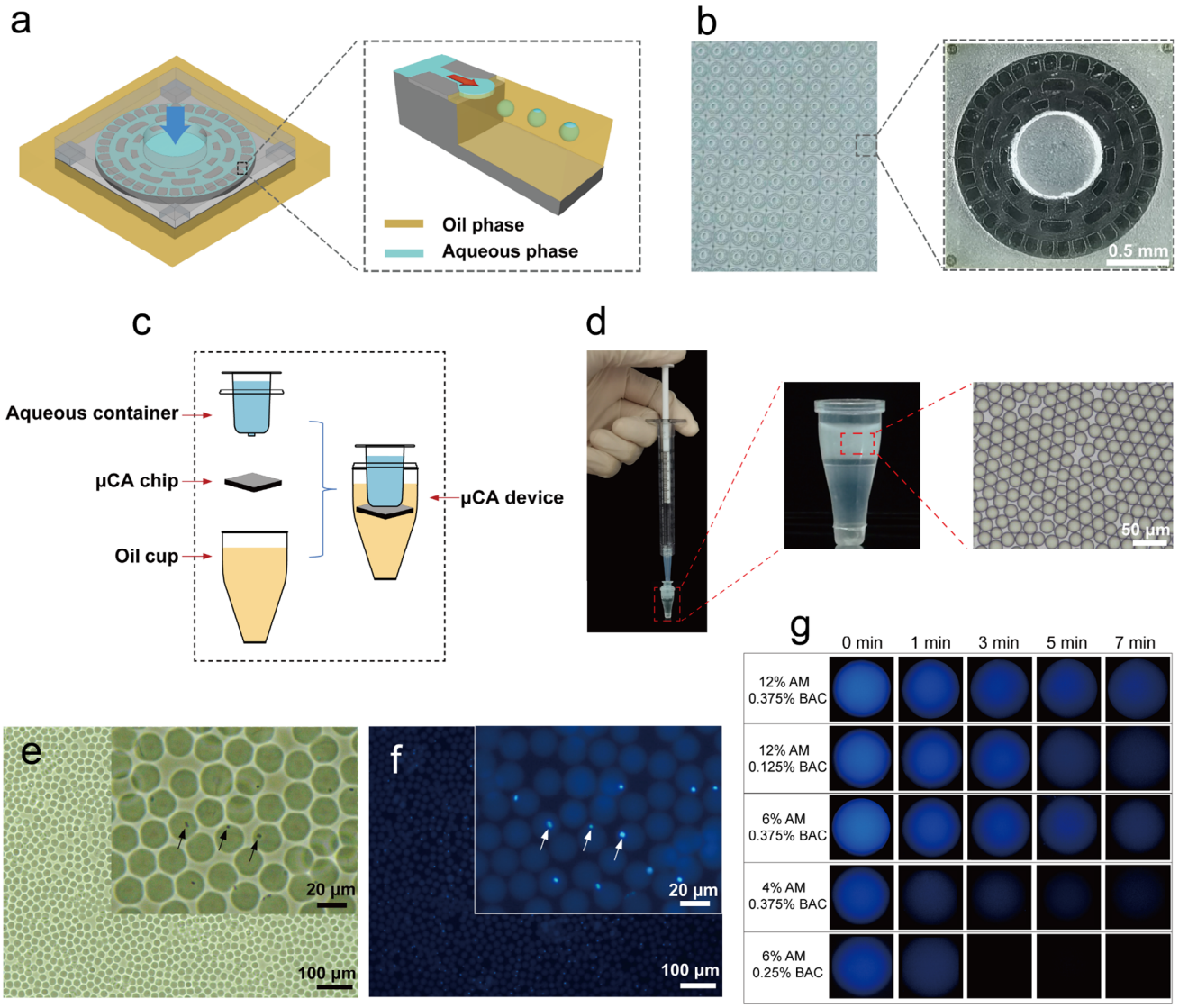


**Figure 2.** Design and components of the μCA device and production of smDHBs. a) 3D image of the μCA chip. The aqueous phase is injected into the center of the chip (blue arrow), flows through the microchannel array on the chip, and is ejected from nozzles on the sides of the chip to form droplets through step emulsification (red arrow). b) Image of the μCA chips etched on a 6 in. silicon wafer, with a magnified microscopic view showing the microchannels. c) Schematic diagram of the μCA device, including its components: the aqueous phase container, the μCA chip and the oil cup. d) Syringe assembled with the μCA device for rapid droplet production. Microscopic image shows uniform droplet size. e,f) Microscopic brightfield and fluorescence images of single *Escherichia coli* encapsulated in smDHBs produced by the μCA device, stained with DAPI. g). Diffusion efficiency of ≈100 kDa molecules in polyacrylamide hydrogels at varying concentrations.

device (Table S1, Supporting Information). Furthermore, the μCA device can be integrated with other detection technologies for biomedical analysis, such as nanopore technology to achieve fast single-molecule detection of biomarkers.[29]

To achieve single-cell encapsulation in smDHBs, we used the Poisson distribution model described by Zilionis et al. to adjust the microbial concentration in the hydrogel solution, ensuring that each smDHB contained at most one microbe.[30] During validation of smDHBs production, we mixed cultured *Escherichia coli* with a polyacrylamide solution and processed using the μCA device. The encapsulated *Escherichia coli* in smDHBs were observed under the microscope, with nearly all smDHBs containing either 0 or 1 bacterium (Figure 2e,f). We estimated the encapsulation efficiency by calculating the ratio of the final number of encapsulated microbes to the initial microbial input, and the efficiency of this encapsulation process is ≈96.4%. In the library preparation of smGel-seq, reagents and enzymes like M-MLV reverse transcriptase (71 kDa) and terminal transferase (58 kDa) need to penetrate the smDHBs to perform the reactions. To assess the permeability of the polyacrylamide hydrogel beads, we adjusted the concentrations of acrylamide monomer (4–12%) and BAC (0.125–0.375%), using ≈100 kDa molecules as a reference model (Figure 2g). We also tested PEG polymer system for smDHBs preparation, but the library quality was poor compared to

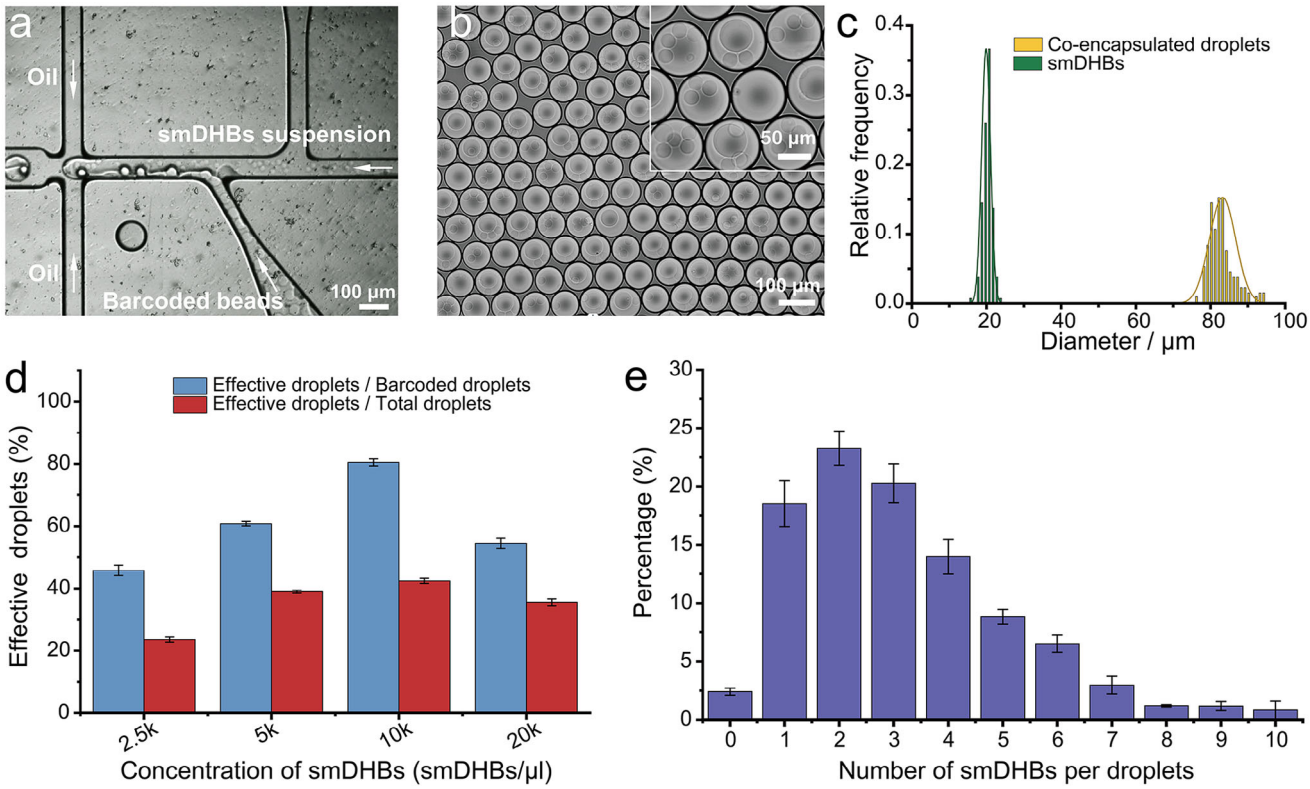


**Figure 3.** Co-encapsulation of smDHBs and barcoded beads by the automated microfluidic platform. a) The microfluidic chip enables the co-encapsulation of smDHBs and barcoded beads within the same droplet. b) Microscope image shows droplets containing barcoded bead and smDHBs. c) Diameter distribution of smDHBs and co-encapsulated droplets. d) Proportion of effective droplets at varying smDHB suspension concentrations. The highest proportion of effective droplets was observed at a concentration of 10 000 smDHBs $\mu L^{-1}$. (Effective droplets are defined as those containing both smDHBs and barcoded beads. Droplets containing barcoded beads are classified as barcoded droplets.) e) Proportion of droplets containing different amounts of smDHBs at a concentration of 10 000 smDHBs $\mu L^{-1}$.

polyacrylamide system (Figure S4, Supporting Information). Based on these tests, we selected 6% acrylamide monomer and 0.25% BAC as the optimal conditions for smDHBs, as molecules diffused most rapidly under this formulation, achieving complete diffusion out of the beads within 3 min. These findings demonstrate that the permeability of polyacrylamide hydrogel beads can be precisely tailored, providing flexibility to accommodate diverse experimental requirements.

## 4. Microfluidic Coencapsulation of smDHBs with Barcoded Beads

To increase the throughput of microbial single-cell sequencing, microfluidic technology was employed to uniquely encode each microbe in smDHBs by co-encapsulating smDHBs and a single barcoded bead within individual droplets. Since the smDHBs generated based on the Poisson distribution result in a significant proportion of empty beads that fail to encapsulate microbes, we aimed to produce droplets that consistently co-encapsulate multiple smDHBs with a single barcoded bead. With smDHBs measuring ≈20 μm in diameter and barcoded beads ≈40 μm, the primary challenge was to reliably generate droplets capable of containing multiple smDHBs and one barcoded bead. To address this problem, we used the automated microfluidic platform VITAcruizer DP400 and chips for the co-encapsulation of smDHBs and barcoded beads. These chips include separate channels for the oil phase, the aqueous phase containing the reagent mix and microbes, and barcoded beads. The aqueous phase channel, with a diameter of 60 μm, allows smDHBs to flow without resistance, which facilitates efficient entry of multiple smDHBs into a single droplet.

We followed the platform's instructions to prepare the aqueous phase by treating smDHBs as microbes. As shown in **Figure 3**a, the smDHB suspension and barcoded beads entered the chip from separate channels and were sheared by the oil phase to form co-encapsulated droplets. However, we observed that smDHBs settled quickly and caused clogging in the channels during droplet generation. To resolve this issue, we formulated the aqueous phase using varying concentrations of density gradient medium. We determined to prepare the aqueous phase as an smDHBs suspension containing 30% density gradient medium for droplet barcoding, as this concentration effectively kept the smDHBs suspended and prevented blockages in the microfluidic channels (Figure S5, Supporting Information). Microscopic examination reveals that most co-encapsulated droplets contain a barcoded bead along with multiple smDHBs (Figure 3b). The droplets generated by this platform and chip exhibited a uniform size distribution, predominantly ranging from 80 and 90 μm (Figure 3c). These results demonstrate the ability of the automated microfluidic system to reliably generate co-encapsulated

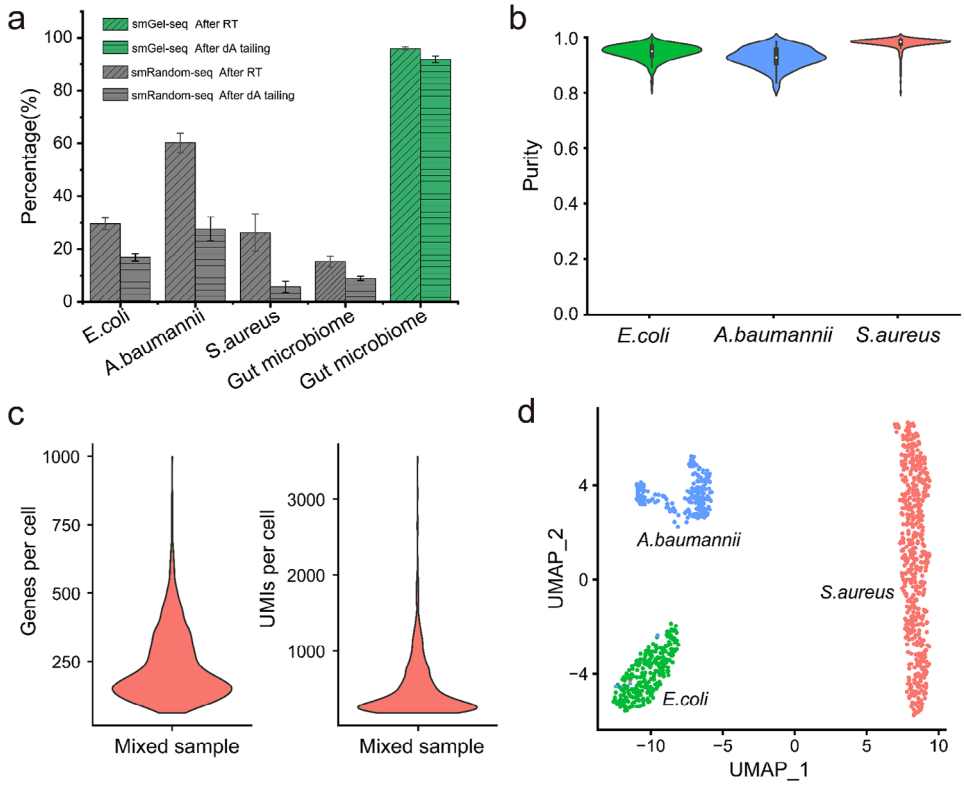


**Figure 4.** Validation of smGel-seq using a three-species mixed bacterial sample and a human gut microbiome sample. a) Microbial recovery rates of smRandom-seq in different samples and smGel-seq in the gut microbiome sample at the end of the reverse transcription and dA tailing reaction. b) Species specificity of UMI in the mixed bacterial sample. The species specificity of *Escherichia coli*, *Acinetobacter baumannii*, and *Staphylococcus aureus* were 95%, 93% and 98%, respectively. c) The three-species mixed bacterial sample showed an average of 220 genes and 486 UMIs per cell. d) UMAP plot showing distinct clusters in the mixed bacterial sample comprising *Acinetobacter baumannii*, *Escherichia coli*, and *Staphylococcus aureus* using smGel-seq.

droplets. To optimize the encapsulation rate, smDHB suspensions with varying concentrations were tested alongside barcoded beads. The highest encapsulation rate was observed at an smDHB concentration of 10 000 smDHBs $\mu L^{-1}$, with higher or lower concentrations leading to reduced efficiency (Figure 3d and Figure S6, Supporting Information). At this optimal concentration, the distribution of smDHBs in droplets was analyzed. The number of smDHBs per droplet ranged from 0 to 10, with 97.6% of droplets containing at least one smDHB (Figure 3e). This range ensures single-microbe encapsulation in droplets, balancing the number of recovered microbes with the risk of dual-cell contamination. Most of droplets (84.9%) contained between 1 and 5 smDHBs, while only 12.7% contained more than 6 smDHBs.

## 5. Evaluating the Performance of smGel-seq

The smGel-seq library preparation process was developed from smRandom-seq, which was introduced in our previous work.[17] The primary steps of smRandom-seq include fixation, cell wall digestion, reverse transcription, dA tailing, and droplet barcoding, with no centrifugation required after the droplet barcoding. To validate smGel-seq, we compared the sample recovery rates of smRandom-seq and smGel-seq. Following multiple centrifugation steps during the reverse transcription and dA tailing reaction of smRandom-seq, we quantified the recovery rate of *Escherichia coli*, *Acinetobacter baumannii*, *Staphylococcus aureus*, and clinical gut microbiome samples. The results revealed significant microbial loss with smRandom-seq, with recovery rates falling below 30% (**Figure** 4a). Notably, the extent of microbial loss varied between samples: *Staphylococcus aureus* exhibited the lowest recovery rate at 5.7%, *Escherichia coli* had a recovery rate of 16.8%, while *Acinetobacter baumannii* showed the highest recovery rate at 27.5%. These findings demonstrate that smRandom-seq is unable to mitigate the quantitative biases introduced during the experimental process. We further prepared the gut microbiome sample in smDHBs to assess the recovery rate of smGel-seq. Without hydrogel encapsulation, the inherent small size of microbes leads to substantial loss during multiple centrifugation steps, yielding only 8.8% recovery efficiency for the gut microbiome sample. In contrast, the smGel-seq method addresses this limitation through hydrogel encapsulation of single microbes, achieving a remarkable recovery rate of 91.8%. This significant improvement is attributed to the formation of relatively large (≈20 µm), uniform hydrogel beads that were not easy to be lost during centrifugation, thereby reducing microbial loss during processing (Figure 4a). This result underscores the significant advantage of smGel-seq in microbiome sample recovery.

Traditional high-throughput mscRNA-seq requires tens of millions of microbial inputs, making it unsuitable for clinical microbiome samples with low microbial content. To evaluate the performance, we applied smGel-seq to a three-species mixed

bacterial sample containing 0.5 million microbes, which is 20 times fewer than required for smRandom-seq. The mixed bacterial sample included *Escherichia coli*, *Acinetobacter baumannii*, and *Staphylococcus aureus*. Sequencing data confirmed the ability of smGel-seq to distinguish these species in pooled sample. Each species demonstrated high UMI (unique molecular identifier) specificity: *Escherichia coli* (95%), *Acinetobacter baumannii* (93%), and *Staphylococcus aureus* (98%) (Figure 4b). At a sequencing depth of 1487 reads per cell, we identified a total of 1059 microbes, with an average of 220 genes and 486 UMIs per cell (Figure 4c). The uniform manifold approximation and projection (UMAP) plot showed that these different species of bacteria were clustered separately, including 318 *Escherichia coli*, 110 *Acinetobacter baumannii* and 549 *Staphylococcus aureus* (Figure 4d). For individual species, we detected an average of 117, 173, and 291 genes per cell for *Escherichia coli*, *Acinetobacter baumannii*, and *Staphylococcus aureus*, respectively, along with average UMI counts of 319, 295, and 647 per cell (Figure S7, Supporting Information). These results demonstrate that smGel-seq achieves a performance level comparable to traditional high-throughput mscRNA-seq methods, even with significantly lower microbial input.[12,13,16,17]

## 6. The Application of smGel-seq in Clinical Microbiome Samples

We further evaluated the applicability of smGel-seq using a clinical gut microbiome sample, which is characteristic for its sample complexity and microbial heterogeneity.[31,32] At a sequencing depth of 1459 mean reads per cell, we obtained ≈8000 microbes using smGel-seq with a microbial input of only 0.5 million, which is 20 times fewer than what is required for smRandom-seq. The average UMIs per cell were 349, and the average number of genes per cell was 73 (**Figure 5a**). From the clinical gut microbiome sample, we detected 38 species, 8 of which had abundances exceeding 1% abundant. After filtering out low-quality barcodes and those with species abundance below 1%, the top three most abundant bacterial species identified were *Neobittarella massiliensis* (61.64%), *Bacteroides xylanisolvens* (17.14%), and *CAG-81 sp900066785* (12.17%) (Figure 5b). To validate the abundant species detected by smGel-seq, another clinical gut microbiome sample was analyzed using both smGel-seq and metagenomic sequencing. Despite the differences in the number of species between the two methods, the relative abundances of overlapping species showed positive correlation ($R = 0.68$, $p = 0.021$; Figure S8, Supporting Information). We utilized UMAP for dimensionality reduction to cluster the gut microbiome, resulting in the formation of 11 cell clusters. Subsequent taxonomic annotation revealed that these clusters corresponded to 8 different bacterial species included *Neobittarella massiliensis*, *Bacteroides xylanisolvens*, *CAG-81 sp900066785*, *Phocaeicola dorei*, *Escherichia coli_D*, *Enterocloster sp001517625*, *Bacteroides ovatus*, and *Parabacteroides distasonis*, with each species forming distinct clusters (Figure 5c). On average, these species exhibited 47, 42, 46, 99, 107, 72, 33, and 38 genes per cell and 289, 289, 359, 207, 216, 175, 272, and 219 UMIs per cell, respectively (Figure S9, Supporting Information). We performed additional analysis at the species level, identifying three distinct functional subpopulations of *Neobittarella massiliensis* through dimensionality reduction clustering and differential gene expression analysis (Figure S10, Supporting Information). Subpopulation 0 exhibits enhanced ribosomal RNA synthesis, indicating that these cells are in a rapid growth state with active protein synthesis. Subpopulation 1 shows elevated expression of various molecular chaperones, suggesting a crucial role in protein quality control and folding regulation, particularly in response to heat stress and in maintaining protein homeostasis. Subpopulation 2 displays diverse functionalities, including antibiotic efflux, energy metabolism, DNA repair, and stress response, highlighting its key role in environmental adaptation and metabolic regulation.

The lung microbiome plays a crucial role in the pathogenesis and progression of various respiratory diseases.[33] Sputum, a widely utilized substitute for lung microbiome research, holds significant clinical value for diagnosis and treatment.[34] While microbial heterogeneity in sputum cannot be resolved using metagenomic or meta-transcriptomic sequencing, mscRNA-seq offers the potential to address this limitation.[16] However, microbial single-cell sequencing of sputum microbiome samples has not been achieved due to technical challenges, including low microbial biomass, contamination with large amounts of human genomic DNA, and the difficulty of isolating microbes from a complex matrix.[33,35] We developed a method that simultaneously uses DTT to liquefy sputum during fixation, enabling effective microbial separation for compatibility with smGel-seq, thus facilitating high-throughput microbial single-cell RNA sequencing in sputum samples. Using this method, we applied smGel-seq to a clinical sputum microbiome sample containing ≈280 000 microbes, which is 35 times fewer than required for smRandom-seq. Clinical laboratory culture results from the hospital identified *Acinetobacter baumannii*, which was resistant to multiple antibiotics, such as imipenem, meropenem, co-trimoxazole, and ceftazidime. Consistently, sequencing data aligned to the *Acinetobacter baumannii* genome with a mapping rate of 94.7%, confirming the laboratory findings. At a sequencing depth of 275 mean reads per cell, we detected 4604 cells, with averages of 70 genes and 92 UMIs per cell (Figure 5d).

UMAP clustering of the sequencing data revealed two distinct subpopulations: subpopulation 1 (7%) and subpopulation 0 (93%) (Figure 5e). To investigate differences between the two subpopulations, we performed differential gene expression analysis and functional annotation of the differentially expressed genes (DEGs). The DEGs of subpopulation 0 and subpopulation 1 showed distinct functional differences (Figure 5e). Subpopulation 0 DEGs were primarily associated with sulfur and nitrogen metabolism, suggesting a focus on energy harnessing through specific metabolic pathways (Figure 5f). In contrast, subpopulation 1 DEGs were enriched in functions related to membrane protein expression, ribosomal protein synthesis, and broad metabolic activities (Figure 5f). The broad metabolic capacity and ribosomal proteins synthesis of subpopulation 1 likely confer a survival advantage, enabling rapid growth and adaptation to variable environments. The high expression of membrane proteins may enhance microbial survival under antibiotic pressure and contribute to pathogenicity. For instance, the outer membrane protein OmpA, a key virulence factor of *Acinetobacter baumannii*, involve in bacterial biofilm formation, antibiotic resistance, and host cell adhesion and invasion.[36,37] Cation diffusion fa-

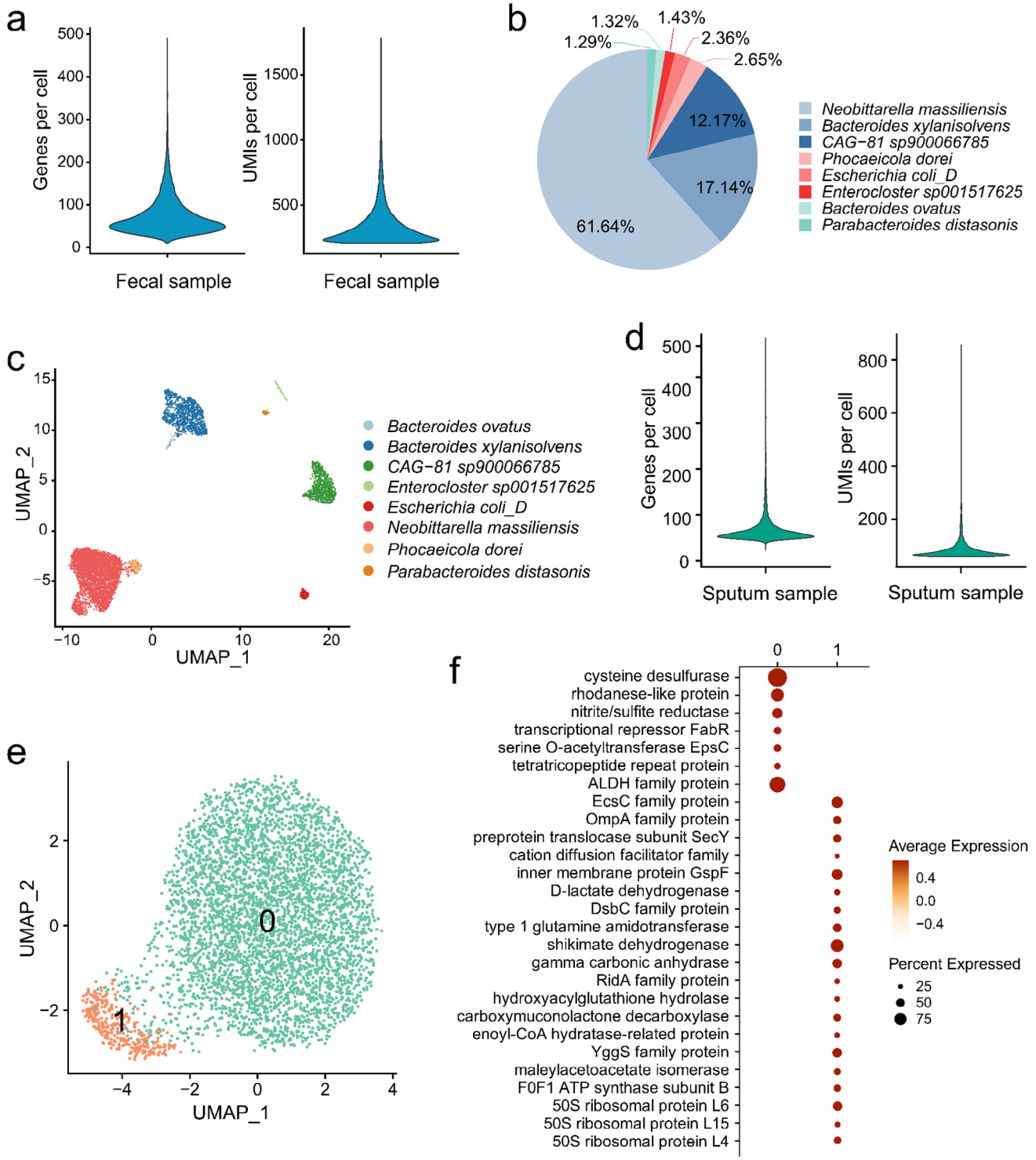


**Figure 5.** Application of smGel-seq in clinical microbiome samples. a) The average number of genes and UMIs detected in the clinical gut microbiome sample was 73 and 349, respectively. b) The proportion of bacterial species with an abundance of more than 1% in the clinical gut microbiome sample. c) UMAP plot of the clinical gut microbiome sample using smGel-seq, with clusters assigned to eight species based on species annotation results. d) The average number of genes and UMIs in the clinical sputum microbiome sample was 70 and 92, respectively. e) UMAP plot of the clinical sputum microbiome sample using smGel-seq, colored to represent subpopulations. f) Dot Plot of DEGs in the clinical sputum microbiome sample across subclusters with functional annotation.

cilitator (CDF) transmembrane proteins, which transport divalent metal cations, participate in resistance of heavy metal antimicrobial agents used in medical therapy.[38,39] The inner membrane protein GspF has been demonstrated to enhance lung colonization efficiency and virulence of *Acinetobacter baumannii*.[40] These findings suggest that subpopulation 1 may have a competitive advantage under host defenses and environmental stress, potentially threatening host health due to its heightened adaptability, antibiotic resistance, and virulence. These results highlight the potential of our method for clinical applications, aiding precise diagnostics and treatment by elucidating mechanisms of pathogenicity and resistance within specific subpopulations of pathogenic species.

## 7. Conclusion

In this work, we developed smGel-seq, a high-throughput microbial single-cell RNA sequencing method characterized by low microbial input, minimal loss, reduced bias, and high sample compatibility. To enable the convenient and rapid generation of hydrogel beads that encapsulate microbes, we invented the μCA device, which is conducive to the wide application of smGel-seq in microbiome research. Additionally, we optimized an automated microfluidic platform that co-encapsulates smDHBs and barcoded beads, significantly increasing throughput by barcoding individual microbes in droplets. Compared to smRandom-seq, smGel-seq significantly improved microbial recovery rate from 8.8% to 91.8% in the human gut microbiome sample. When applied to the clinical gut microbiome sample, smGel-seq effectively distinguished different species within complex microbial communities. Furthermore, we first achieved high-throughput microbial RNA sequencing of clinical sputum microbiome samples by smGel-seq, revealing functional heterogeneity among subpopulations of pathogenic bacterial species, which may provide valuable data for precision diagnostics and treatment. smGel-seq has demonstrated its potential for widespread application in microbiome research and clinical diagnostics, paving the way for high-throughput microbial single-cell RNA sequencing (mscRNA-seq) across diverse microbiome samples.

## 8. Experimental Section

*Materials and Reagents*: 1H,1H,2H,2H-perfluorooctyltrichlorosilane, hexane solvent, Span-80, lysozyme, acrylamide solution (40% w/v), isopropyl alcohol, lysostaphin, methanol, tetramethylethylenediamine, ammonium persulfate, density gradient medium (OptiPrep), and dithiothreitol (DTT) were procured from Sigma. 1H,1H,2H, 2H-perfluorooctanol (PFO) and bis-acryloyl cystamine (BAC) were ordered from Adamas-beta. 4% paraformaldehyde (PFA), NaCl, KCl, $NaH_2PO_4$, $KH_2PO_4$, and PEG8000 were obtained from Sangon Biotech (Shanghai, China). Carrier oil (008-FluoroSurfactant-2wtH-50G) was purchased from were purchased from RAN Biotechnologies. HFE-7500 oil (3M Novec 7500 Engineered Fluid) was ordered from 3M. The VAHTS Universal DNA Library Prep Kit for Illumina V3 (ND607-03/04) was supplied by Vazyme. All reagents used in the smGel-seq library preparation process that were not mentioned above were ordered from M20 Genomics.

*Fabrication of μCA Chip*: The μCA chip was fabricated based on previous work.[41] The photomask for the μCA chip was designed using AutoCAD software. The AZ5214 photoresist was applied to a 6 in. silicon wafer via spin-coating (600 rpm for 5 s, 4000 rpm for 30 s) and prebaked at 95 °C for 90 s. Then the wafer was exposed to UV light through the photomask on a SUSS MA6 Mask Aligner. After exposure, the wafer was rinsed for 45 s in a 2.38% developer solution and post-baked at 100 °C for 2 min. Following the photolithography process, the pattern on the silicon wafer was further defined through inductively coupled plasma (ICP) etching, using the parameters from our previous work.[28] A glass with a cylindrical through-hole in the center was bonded to the wafer. Over 2000 μCA chips were produced on a 6 in. silicon wafer, and individual chips were obtained through laser cutting.

*Hydrophobic Treatment of the μCA Chip Surface*: Hydrophobic treatment of μCA chip surface is essential for the stable generation of droplets. The μCA chips were immersed in piranha solution (the volume ratio of $H_2O_2$ to $H_2SO_4$ is 3:1) and ultrasonically cleaned for 10 min. Following this, the μCA chips were rinsed with $ddH_2O$ and dried at 70 °C for 6 h. Next, the chips were treated with oxygen plasma and then placed in a vacuum desiccator containing a bottle of opened 1H,1H,2H,2H-perfluorooctyltrichlorosilane for 1 h. The chips were placed on a hot plate at 120 °C for 5 min. Finally, the chips were washed again with isopropyl alcohol and $ddH_2O$, and dried in a natural environment.

*Preparation of Sample*: For the three-species mixed bacterial sample, *Escherichia coli* BW25113, *Acinetobacter baumannii* ATCC17978, and *Staphylococcus aureus subsp. Aureus* SA268 were provided by Sir Run Run Shaw Hospital, Zhejiang University School of Medicine. These three bacteria were cultured on LB agar plates for 24 h, after which single colonies were selected and inoculated into LB liquid medium for overnight incubation at 37 °C, respectively. 500 μL of each cultured bacterial suspension was resuspended in 4% PFA and fixed overnight at 4 °C. The fixed bacteria were counted under a microscope and then mixed in equal numbers to create a microbial suspension.

The clinical microbiome samples were collected from the First Affiliated Hospital of Zhejiang University. The study protocol was approved by the Ethics Committee of the First Affiliated Hospital, Zhejiang University School of Medicine, China (2021IIT A0239). All the participants provided written informed consent. Upon collection, the clinical gut microbiome sample was immediately resuspended in 4% PFA for fixation, and the clinical sputum microbiome sample was immediately resuspended in PFA-DTT buffer (4% PFA, 1 mg $mL^{-1}$ DTT, 0.2% PEG8000, 0.39 mg $mL^{-1}$ NaCl, 0.01 mg $mL^{-1}$ KCl, 0.056 mg $mL^{-1}$ $NaH_2PO_4$, 0.01 mg $mL^{-1}$ $KH_2PO_4$) for fixation and liquefaction, then kept at 4 °C and rotated overnight. After fixation, impurities and host cells were removed from these clinical microbiome samples by filtration at 40 μm and centrifuging twice or more times for 3 min at 500 *g*, 4 °C. Then all samples were centrifuged at 3900 *g*, 4 °C for 15 min and washed with PBS. The microbial suspension was counted under a microscope.

*smDHBs Generation*: A 50 μL polyacrylamide solution was prepared, including 7.5 μL acrylamide solution, 2.5 μL bis-acryloyl cystamine in methanol (5% w/v), 2.5 μL ammonium persulfate (10% w/v), 15 μL PBS and 22.5 μL fixed microbial suspension (0.15–1 million microbes). The 50 μL polyacrylamide solution was loaded into an aqueous container and 150 μL carrier oil was loaded into an oil cup. A μCA chip was assembled with the aqueous container and oil cup to form a μCA device, in which the μCA chip was immersed in oil. Then the container was connected with a 1 mL syringe. Manual pushing of the syringe generates pressure that drives the aqueous phase into the microchannels of the μCA chip, completing the formation of droplets within 30 s. 4 μL tetramethylethylenediamine (TEMED) was mixed with 200 μL of carrier oil in a 1.5 mL centrifuge tube, and all the droplets were transferred into this tube. The droplets were incubated at 37 °C for 1 h for gelation. After removing of bottom oil by a pipette, the droplets were broken using 200 μL PFO in HFE-7500 (20% v/v) and all the oil phase was removed. Finally, the smDHBs were washed twice by 1 mL Span-80 in hexane solvent (1% v/v) and three times by PBS buffer at 1000 g for 1 min.

*smGel-seq Library Preparation*: The library preparation of smGel-seq is based on our previous work of smRandom-seq and smRandom-seq2.[17,42] All smDHBs were resuspended in 250 μL PBS with 0.04% Tween-20. Then the smDHBs were treated with lysozyme (2.5 mg $mL^{-1}$) and lysostaphin (0.0125 mg $mL^{-1}$) to lyse cell wall at 37 °C for 15 min. After lysis, smDHBs were immediately washed three times with PBS with

RNase inhibitor. Reactions of reverse transcription and dA tailing were performed in situ by reverse transcription kit. The reverse transcription mix was prepared, including 4 µL reverse transcriptase, 18 µL 5× RT buffer (without DTT), 4.5 µL RNase inhibitor, 4.5 µL dNTP Mix (10 mM each), 49.5 µL smDHBs and 9 µL random primer (10 µM). The mix was incubated in a thermal cycler with twelve cycles of temperature gradient annealing from 8 to 42 °C, followed by a 30 min incubation at 42 °C. After the reaction, smDHBs were washed five times with PBST buffer (PBS with 0.05% Tween-20). The dA reaction was then carried out by adding 1 µL TdT enzyme, 1 µL 100 mM dATP, 10 µL 10× TdT buffer and 10 µL $CoCl_2$ to the smDHBs, followed by the addition of PBS to adjust the final volume to 100 µL. After incubating the mixture at 37 °C for 30 min, the smDHBs were washed three times with PBST buffer.

For droplet barcoding of single microbes, co-encapsulation of smDHBs and barcoded beads was performed on VITAcruizer DP400 platform (M20 Genomics, Hangzhou, China). smDHBs were counted under a microscope. Then smDHBs suspension was prepared by mixing 30% density gradient solution, DNA extension reaction mix, and smDHBs with final concentration of 10 000 smDHBs $\mu L^{-1}$. Then barcoded beads and the smDHBs suspension were co-encapsulated into droplets using VITACruiser. The droplets were incubated through a sequence of temperatures steps: 37 °C for 1 h, 50 °C for 30 min, 60 °C for 30 min, and 75 °C for 20 min. Then the droplets were broken using PFO in HFE-7500 (20% v/v), resulting in the separation of the oil phase and the aqueous phase. In the aqueous phase, a final concentration of 10 mM DTT was added to dissolve the smDHBs and release all the cDNAs within 3 min. Following this, the aqueous phase was mixed with Ampure XP beads to purified cDNAs. The cDNAs were enriched by PCR amplification and then purified again with Ampure XP beads.

The VAHTS Universal DNA Library Prep Kit for Illumina V3 was used to construct the cDNAs into a sequencing library. The quality and quantity of the cDNAs were measured by Qsep100 DNA Fragment Analyzer and Qubit 2.0. A reaction mixture was prepared, containing 50 ng cDNAs, end-repair enzymes, buffer, and nuclease-free water, and incubated 30 min at 30 °C. After inactivation at 65 °C for 30 min, the working adaptor and ligation enzymes are added and the mixture was incubated at 20 °C for 15 min to facilitate ligation. AMPure XP beads were used for DNA size selection to enrich the target fragment range. The quality and quantity of the cDNAs were measured by Qsep100 DNA Fragment Analyzer and Qubit 2.0. The library was then sequenced on the NovaSeq 6000 platform with the S4 Reagent Kit, utilizing paired-end reads of 150.

*Data Analysis*: For the three-species mixed bacterial sample, the initial processing of raw sequencing data was conducted by removing the primer sequence and trimming of poly(dA) tail. Within each Read1, the UMI consisting of 8 nucleotides and cell-specific barcode consisting of 20 nucleotides were identified and extracted. Sequenced barcodes were merged when they could be uniquely mapped to an accepted barcode, allowing for a Hamming distance of no more than 2 nucleotides. Read2 was mapped to the merged genome of *E. Coli* (GCF_000750555.1), *A. baumannii* (GCF_902728005.1), and *S. Aureus* (GCF_000737615.1) to generate the gene expression matrix using STAR (v.2.7.10a),[43] retaining only the uniquely mapped reads. The gene expression matrix was further analyzed by the R package Seurat (v.4.3.0).[44] The raw gene expression matrix data were imported and a Seurat object was constructed, with the criterion of including genes detected in at least one cell. Data normalization was performed by NormalizeData function, and 6000 most variable genes were identified using FindVariableFeatures. The most variable genes were z-scored using ScaleData function and applied Principal Component Analysis (PCA) for reducing the dimensionality of the transcriptomic space. Using FindNeighbors and FindClusters functions, cells were clustered based on their transcriptomic similarity with dimensions 1–15. The clusters were then further visualized using uniform manifold approximation and projection (UMAP) with a minimum distance of 0.3 and a resolution of 0.03. Subsequently, FindAllMarkers function was utilized to identify differentially expressed genes specific and annotation to each cluster and annotate them, considering an average $\log_2$ fold change.

For the human gut microbiome sample, Kraken2 was used, a K-mer-based taxonomic classification tool, to analyze each read of every barcode by utilizing UHGG (v2.0.1)[45] gut microbiome genomic database as a reference. The metagenomic analysis process was referred and the software tool Bracken was utilized to correct the reads. Bracken employs Bayesian inference to combine Kraken's preliminary classification results with k-mer frequency distribution, enabling the identification of reads at the species level. After calculating the read proportions of each species in each barcode, each barcode was annotated as the species with the highest proportion. Then the data underwent identical processing to the three-species mixed bacterial sample for primer removal, poly(dA) tail trimming, UMI and barcode extraction, and barcode merging. Read2 was mapped to whole UHGG (v2.0.1)[45] gut microbiome genome using STAR (v.2.7.10a)[43] to generate the gene expression matrix. Uniquely mapped reads were retained to tally UMIs for each barcode. Low-quality barcodes and species with few cells based on a threshold of 1% total barcodes for the downstream analysis were filtered out.[42] The gene expression matrix was further analyzed by the R package Seurat (v.4.3.0)[44] for dimensional reduction.

For the clinical sputum microbiome sample, the initial processing of the raw sequencing data was consistent with that of the three-species mixed bacterial sample, except that the read2 was aligned to the genome of *A. baumannii* (GCF_000372585.2). The generated gene expression matrix was analyzed using the R package Seurat (v.4.3.0) for visualized with UMAP dimensionality reduction, analysis of differentially expressed genes, and functional annotation of differentially expressed genes with 1000 variable genes.

## Supporting Information

Supporting Information is available from the Wiley Online Library or from the author.

## Acknowledgements

The project was supported by the National Natural Science Foundation of China (No. 32200073, Y.W., No. 32250710678, Y.W., and No. 52203282, Z.T.), Leading Innovative and Entrepreneur Team Introduction Program of Zhejiang (No. 2021R01012, Y.W.), "Pioneer" R&D programs of Zhejiang Province (No. 2024C03005, Y.W.), and Key R&D Program of Zhejiang (No. 2024SSYS0022, Y.W.), and Zhejiang Provincial Natural Science Foundation of China (LY23B040002, Z.T.). The authors thank for the technical support by the core facilities of Zhejiang University and Liangzhu Laboratory.

## Conflict of Interest

Yongcheng Wang is a co-founder of M20 Genomics. Yongcheng Wang, Yuting Wang, and Zhengmin Tang have filed a patent related to this work.

## Data Availability Statement

The data that support the findings of this study are available from the corresponding author upon reasonable request.

## Keywords

microbial single-cell RNA-seq technology (mscRNA-seq), microbiome, smDHBs, smGel-seq

Received: January 8, 2025
Revised: March 21, 2025
Published online:

[1] E. Rackaityte, S. V. Lynch, *Nat. Commun.* **2020**, *11*, 5256.
[2] P. W. O'Toole, M. Paoli, *Nat. Rev. Microbiol.* **2023**, *21*, 624.
[3] N. Aggarwal, S. Kitano, G. R. Y. Puah, S. Kittelmann, I. Y. Hwang, M. W. Chang, *Chem. Rev.* **2023**, *123*, 31.
[4] C. Averill, M. A. Anthony, P. Baldrian, F. Finkbeiner, J. van den Hoogen, T. Kiers, P. Kohout, E. Hirt, G. R. Smith, T. W. Crowther, *Nat. Microbiol.* **2022**, *7*, 1717.
[5] V. Llorens-Rico, J. A. Simcock, G. R. B. Huys, J. Raes, *Cell* **2022**, *185*, 2725.
[6] E. Bauer, C. C. Laczny, S. Magnusdottir, P. Wilmes, I. Thiele, *Microbiome* **2015**, *3*, 55.
[7] F. Lan, J. Saba, Y. Qian Ross, T. Landick, R. V. O. S., *Sci. Adv.* **2023**, *9*, adg5476.
[8] Y. Jiang, X. Xiong, J. Danska, J. Parkinson, *Microbiome* **2016**, *4*, 2.
[9] Y.-L. Ying, Z.-L. Hu, S. Zhang, Y. Qing, A. Fragasso, G. Maglia, A. Meller, H. Bayley, C. Dekker, Y.-T. Long, *Nat. Nanotechnol.* **2022**, *17*, 1136.
[10] M.-Y. Li, J. Jiang, J.-G. Li, H. Niu, Y.-L. Ying, R. Tian, Y.-T. Long, *Nat. Methods* **2024**, *22*, 241.
[11] H. Meng, T. Zhang, Z. Wang, Y. Zhu, Y. Yu, H. Chen, J. Chen, F. Wang, Y. Yu, X. Hua, Y. Wang, *Angew. Chem., Int. Ed.* **2024**, *63*, 202400538.
[12] P. Ma, H. M. Amemiya, L. L. He, S. J. Gandhi, R. Nicol, R. P. Bhattacharyya, C. S. Smillie, D. T. Hung, *Cell* **2023**, *186*, 877.
[13] S. B. Blattman, W. Jiang, P. Oikonomou, S. Tavazoie, *Nat. Microbiol.* **2020**, *5*, 1192.
[14] F. Imdahl, E. Vafadarnejad, C. Homberger, A. E. Saliba, J. Vogel, *Nat. Microbiol.* **2020**, *5*, 1202.
[15] J. W. Bagnoli, C. Ziegenhain, A. Janjic, L. E. Wange, B. Vieth, S. Parekh, J. Geuder, I. Hellmann, W. Enard, *Nat. Commun.* **2018**, *9*, 2937.
[16] A. Kuchina, L. M. Brettner, L. Paleologu, C. M. Roco, A. B. Rosenberg, A. Carignano, R. Kibler, M. Hirano, R. W. DePaolo, G. Seelig, *Science* **2021**, *371*, aba5257.
[17] Z. Xu, Y. Wang, K. Sheng, R. Rosenthal, N. Liu, X. Hua, T. Zhang, J. Chen, M. Song, Y. Lv, S. Zhang, Y. Huang, Z. Wang, T. Cao, Y. Shen, Y. Jiang, Y. Yu, Y. Chen, G. Guo, P. Yin, D. A. Weitz, Y. Wang, *Nat. Commun.* **2023**, *14*, 5130.
[18] I. Lameira, A. S. Pinto, Â. Lima, C. A. Muzny, N. Cerca, *J. Microbiol. Methods* **2024**, *219*, 106895.
[19] J. Lloyd-Price, G. Abu-Ali, C. Huttenhower, *Genome Med.* **2016**, *8*, 51.
[20] S. Liu, N. Zheng, J. Wang, S. Zhao, *Front. Microbiol.* **2024**, *15*, 1376994.
[21] Y. Wang, T. Cao, J. Ko, Y. Shen, W. Zong, K. Sheng, W. Cao, S. Sun, L. Cai, Y. L. Zhou, X. X. Zhang, C. Zong, R. Weissleder, D. Weitz, *Adv. Sci.* **2020**, *7*, 1903463.
[22] J. Lou, D. J. Mooney, *Nat. Rev. Chem.* **2022**, *6*, 726.
[23] A. Rakszewska, R. J. Stolper, A. B. Kolasa, A. Piruska, W. T. Huck, *Angew. Chem., Int. Ed.* **2016**, *55*, 6698.
[24] W. Jang, J. Kim, S. J. Mun, S. M. Kim, K. W. Bong, *Biomedicines* **2021**, *9*, 848.
[25] Y. H. Roh, R. T. Morales, E. Huynh, U. Chintapula, D. E. Reynolds, R. J. Agosto-Nieves, D. Oh, A. J. Seiner, J. Lim, C. B. Rodell, J. Ko, *Small* **2025**, *21*, 2407809.
[26] K. Ide, Y. Nishikawa, T. Maruyama, Y. Tsukada, M. Kogawa, H. Takeda, H. Ito, R. Wagatsuma, R. Miyaoka, Y. Nakano, K. Kinjo, M. Ito, M. Hosokawa, K. Yura, S. Suda, H. Takeyama, *Microbiome* **2022**, *10*, 220.
[27] F. Lan, J. Saba, T. D. Ross, Z. Zhou, K. Krauska, K. Anantharaman, R. Landick, O. S. Venturelli, *Nat. Methods* **2024**, *21*, 228.
[28] Z. Tang, F. Lv, D. E. Reynolds, S. Zhang, S. Zheng, J. Ko, Y. Chen, Y. Wang, *Lab Chip* **2023**, *23*, 2758.
[29] L.-L. Zhang, C.-B. Zhong, T.-J. Huang, L.-M. Zhang, F. Yan, Y.-L. Ying, *Chem. Sci.* **2024**, *15*, 8355.
[30] R. Zilionis, J. Nainys, A. Veres, V. Savova, D. Zemmour, A. M. Klein, L. Mazutis, *Nat. Protoc.* **2017**, *12*, 44.
[31] Z. Huang, K. Liu, W. Ma, D. Li, T. Mo, Q. Liu, *Front. Microbiol.* **2022**, *13*, 1018594.
[32] D. Liang, R. K.-K. Leung, W. Guan, W. W. Au, *Gut Pathog.* **2018**, *10*, 3.
[33] J. G. Natalini, S. Singh, L. N. Segal, *Nat. Rev. Microbiol.* **2023**, *21*, 222.
[34] S. A. Whiteside, J. E. McGinniss, R. G. Collman, *J. Clin. Invest.* **2021**, *131*, 150473.
[35] L. Terranova, M. Oriano, A. Teri, L. Ruggiero, C. Tafuro, P. Marchisio, A. Gramegna, M. Contarini, E. Franceschi, S. Sottotetti, L. Cariani, A. Bevivino, J. D. Chalmers, S. Aliberti, F. Blasi, *Int. J. Mol. Sci.* **2018**, *19*, 3256.
[36] D. Scribano, E. Cheri, A. Pompilio, G. Di Bonaventura, M. Belli, M. Cristina, L. Sansone, C. Zagaglia, M. Sarshar, A. T. Palamara, C. Ambrosi, *Commun. Biol.* **2024**, *7*, 948.
[37] D. Nie, Y. Hu, Z. Chen, M. Li, Z. Hou, X. Luo, X. Mao, X. Xue, *J. Biomed. Sci.* **2020**, *27*, 26.
[38] S. F. Alquethamy, F. G. Adams, R. Maharjan, N. N. Delgado, M. Zang, K. Ganio, J. C. Paton, K. A. Hassan, I. T. Paulsen, C. A. McDevitt, A. K. Cain, B. A. Eijkelkamp, *Appl. Environ. Microbiol.* **2021**, *87*, 0171821.
[39] O. Kolaj-Robin, D. Russell, K. A. Hayes, J. T. Pembroke, T. Soulimane, *FEBS Lett.* **2015**, *589*, 1283.
[40] N. M. Elhosseiny, O. M. El-Tayeb, A. S. Yassin, S. Lory, A. S. Attia, *Int. J. Med. Microbiol.* **2016**, *306*, 633.
[41] Z. Tang, D. E. Reynolds, C. Lv, D. Zhang, J. Ko, Y. Wang, *Small Sci.* **2024**, *4*, 2400005.
[42] Y. Shen, Q. Qian, L. Ding, W. Qu, T. Zhang, M. Song, Y. Huang, M. Wang, Z. Xu, J. Chen, L. Dong, H. Chen, E. Shen, S. Zheng, Y. Chen, J. Liu, L. Fan, Y. Wang, *Protein Cell* **2025**, *16*, 211.
[43] A. Dobin, C. A. Davis, F. Schlesinger, J. Drenkow, C. Zaleski, S. Jha, P. Batut, M. Chaisson, T. R. Gingeras, *Bioinformatics* **2013**, *29*, 15.
[44] Y. Hao, S. Hao, E. Andersen-Nissen, W. M. Mauck, S. Zheng, A. Butler, M. J. Lee, A. J. Wilk, C. Darby, M. Zager, P. Hoffman, M. Stoeckius, E. Papalexi, E. P. Mimitou, J. Jain, A. Srivastava, T. Stuart, L. M. Fleming, B. Yeung, A. J. Rogers, J. M. McElrath, C. A. Blish, R. Gottardo, P. Smibert, R. Satija, *Cell* **2021**, *184*, 3573.
[45] A. Almeida, S. Nayfach, M. Boland, F. Strozzi, M. Beracochea, Z. J. Shi, K. S. Pollard, E. Sakharova, D. H. Parks, P. Hugenholtz, N. Segata, N. C. Kyrpides, R. D. Finn, *Nat. Biotechnol.* **2020**, *39*, 105.